

Dynamic conformational changes of extracellular S5–P linkers in the hERG channel

Min Jiang¹, Mei Zhang¹, Innokenty V. Maslennikov², Jie Liu¹, Dong-Mei Wu¹, Yuliya V. Korolkova², Alexander S. Arseniev², Eugene V. Grishin² and Gea-Ny Tseng¹

¹Department of Physiology, Virginia Commonwealth University, Richmond, VA 23298, USA

²Shemyakin-Ovchinnikov Institute of Bioorganic Chemistry, Russian Academy of Sciences, Moscow, 117997 Russia

The hERG channel has an unusually long ‘S5–P linker’ (residues 571–613) that lines the outer mouth of the pore. Previously, we have shown that residues along this S5–P linker are critical for the fast-inactivation process and K⁺ selectivity of the hERG channel. Here we used several approaches to probe the structure of this S5–P linker and its interactions with other domains of the hERG channel. Circular dichroism and NMR analysis of a synthetic hERG S5–P linker peptide suggested that this linker is quite dynamic: its central region (positions 583–593) can be unstructured or helical, depending on whether it is immersed in an aqueous phase or in contact with a hydrophobic environment. Cysteine introduced into positions 583–597 of the S5–P linker can form intersubunit disulphide bonds, and at least four of them (at 584, 585, 588 and 589) can form disulphide bonds with counterparts from neighbouring subunits. We propose that the four S5–P linkers in a hERG channel can engage in dynamic conformational changes during channel gating, and interactions between S5–P linkers from neighbouring subunits contribute importantly to channel inactivation.

(Resubmitted 27 June 2005; accepted after revision 2 September 2005; first published online 8 September 2005)

Corresponding author G.-N. Tseng: Department of Physiology, Virginia Commonwealth University, 1101 E. Marshall Street, Richmond, VA 23298, USA. Email: gtseng@hsc.vcu.edu

Human *ether-à-go-go* related gene (*hERG*) encodes the pore-forming subunit of rapid delayed rectifier (I_{Kr}) channels in human heart (Sanguinetti *et al.* 1995). It has a uniquely fast and voltage-sensitive inactivation process (Spector *et al.* 1996; Smith *et al.* 1996). This fast-inactivation process, along with the slow activation and deactivation rates of the hERG/I_{Kr} channel, creates its inward rectification property (Spector *et al.* 1996): there is little outward current through the hERG/I_{Kr} channels during phase 2 of cardiac action potential due to channel inactivation, but a resurgence of outward current occurs during phase 3 when the hERG/I_{Kr} channels recover from inactivation. This outward hERG/I_{Kr} current during phase 3 of cardiac action potentials serves an antiarrhythmic function by preventing premature depolarization from triggering extrasystole.

The hERG channel shares structural design with other Kv channels. Each functional channel has four subunits, and each subunit is composed of a voltage-sensing domain (S1–S4) and a pore domain (S5–pore loop–S6) (Fig. 1A). hERG differs from many K⁺ channels in having a longer S5–P linker (43 aa *versus* 12–23 aa, Fig. 1B). We have performed a cysteine (Cys) scanning mutagenesis analysis of hERG’s S5–P linker (Liu *et al.*

2002). Cysteines introduced into 14 positions in the centre of the hERG S5–P linker, from 583 to 597 (excluding 595; cysteine substitution at this position produces a non-functional channel) can form disulphide bonds. Disulphide bond formation produces a uniform mutant phenotype: disruption of the fast-inactivation process and the pore’s K⁺ selectivity (Liu *et al.* 2002). Thus, the central portion of the S5–P linker in the hERG channel can engage in interactions with other channel domains, or with its counterparts, to allow disulphide bond formation. Furthermore, its peptide backbone conformation or interaction with other channel domains or counterparts is important for the fast-inactivation process as well as the pore’s K⁺ selectivity.

Among these 14 cysteine substituted mutants, 7 revert to a wild-type (WT)-like phenotype (fast-inactivation and strong K⁺ selectivity) after treatment with dithiothreitol (DTT), which breaks disulphide bonds (Liu *et al.* 2002). Therefore, cysteine substitution *per se* is tolerated at these positions. However, modification of these introduced cysteine side chains by methanethiosulphonate (MTS) reagents markedly reduces the channel conductance or, for G584C, disrupts inactivation as well as K⁺ selectivity (Liu *et al.* 2002). These are classified as ‘intermediate-impact’

positions, as opposed to ‘low-impact’ positions where neither cysteine substitution nor subsequent MTS modification has much impact on the channel function (colour coded blue and black in the hERG sequence in Fig. 1B). The other seven cysteine-substituted mutants maintain the mutant phenotype after DTT treatment. This suggests that side chain properties at these positions are critical for the fast-inactivation process and the pore’s K⁺ selectivity of the hERG channel, so that cysteine substitution is not tolerated. These are designated ‘high-impact’ positions. Position 595 is also a high-impact position. The high-impact positions along the 583–597 segment and those in other regions of the S5–P and P–S6 linkers are colour coded red in the hERG sequence in Fig. 1B.

Why is the central portion of the S5–P linker so critical for the fast-inactivation process and K⁺ selectivity of the hERG channel? Inactivation in the hERG channel is similar to the C-type inactivation in the Shaker channel (Hoshi *et al.* 1991; Smith *et al.* 1996; Herzberg *et al.* 1998):

inactivation results from conformational changes around the selectivity filter that prevent ion conduction through the pore. The channel pore’s selectivity for K⁺ ions is also mainly determined by the selectivity filter (Fig. 1B). In the available K⁺ channel crystal structures (Doyle *et al.* 1998; Jiang *et al.* 2002; Jiang *et al.* 2003), the turrets (corresponding to hERG’s S5–P linker) are immersed in the extracellular solution, making no direct contact with the selectivity filter (Fig. 1C). However, our data described above suggest that this may not be the case for hERG. In this study, we take several approaches to examine the secondary structure of the 583–597 segment and to explore its interaction with other channel domains: (1) circular dichroism (CD) spectral analysis and spatial structure calculations based on nuclear magnetic resonance (NMR) data are used to directly probe the secondary structure and side chain mobility of a synthetic hERG S5–P linker peptide that includes the 583–597 segment and its flanking regions, and (2) site-specific mutations in conjunction with biochemical and electrophysiological analysis are used to

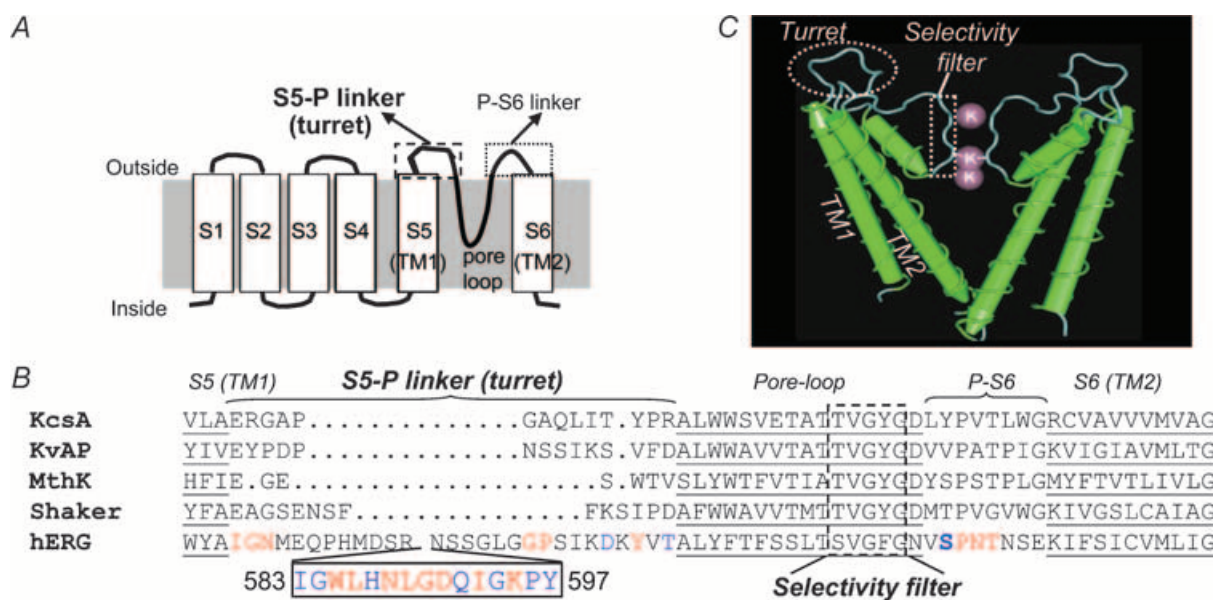


Figure 1. The amino acid sequence lining the outer mouth region of hERG suggests unique structure and function

A, two-dimensional diagram of a voltage-gated K⁺ (Kv) channel subunit, with the following domains marked: transmembrane segments (S1 to S6), pore-loop and the two extracellular linkers lining the outer mouth (S5–P and P–S6 linkers). S5 and S6 correspond to TM1 and TM2 (or outer and inner helices) of 2-transmembrane domain K⁺ channels such as KcsA and MthK, and S5–P linker is equivalent to ‘turrets’ in the K⁺ channel crystal structures. **B**, alignment of amino acid sequences of KcsA, KvAP, MthK, Shaker and hERG from the end of S5 (TM1) to the middle of S6 (TM2). The K⁺ channel signature sequence that lines the selectivity filter is highlighted by a dotted rectangle. The 583–597 segment of hERG’s S5–P linker is shown as an inset. In the hERG sequence, red and blue colours denote high- and intermediate-impact positions based on the effects of cysteine substitution on the channel function (Liu *et al.* 2002). **C**, crystal structure of KcsA, showing 2 diagonal subunits with 3 K⁺ ions coordinated by the selectivity filter. TM1, TM2, turret and selectivity filter are marked.

probe side chain interactions in this segment of an intact channel and how these interactions impact on channel function.

Methods

Circular dichroism (CD) and nuclear magnetic resonance (NMR) spectroscopy of a synthetic hERG S5–P linker peptide

Peptide synthesis. A 25-mer 'hERG S5–P linker' peptide corresponding to hERG residues 578–603 was synthesized by Obrigen (San Diego, CA, USA). The peptide was purified by reverse phase HPLC and composition of the purification product was verified by mass spectroscopy.

CD spectroscopy. Sample of hERG S5–P linker peptide (74 μM) in 4.44 mM diphenylamine carboxylic acid (DPC) (peptide/DPC = 1/60) or in 5.92 mM sodium dodecyl sulphate (SDS) (peptide/SDS = 1/80) was prepared in H_2O and pH was titrated to 3.5. CD spectra were obtained using spectropolarimeter J-715 (Jasco, Easton, MD, USA) in the wavelength range 185–250 nm at 22°C with a 0.02 cm quartz cell.

NMR spectroscopy. NMR sample of 0.6 mM hERG S5–P linker peptide in 10% D_2O or of 0.35 mM peptide in 21 mM DPC (peptide/DPC = 1/60, in 10% D_2O) was used. ^1H NMR spectra (double quantum-filtered correlated spectroscopy (DQF-COSY) (Rance *et al.* 1983), total correlation spectroscopy (TOCSY) (Bax & Davis, 1985) with mixing times (τ_{m}) of 40 and 80 ms, and Overhauser enhancement spectroscopy (NOESY) (Jeener *et al.* 1979) with τ_{m} of 100 and 200 ms) were acquired using a 600 MHz spectrometer (Unity 600, Varian, Palo Alto, CA, USA) at 30°C, pH 3.5. NMR data were processed with VNMR (Varian software), and analysed with the XEASY program (Bartels *et al.* 1995). Proton resonance assignment of hERG S5–P linker peptide in DPC was performed by standard procedure (Wuthrich, 1986) using the XEASY program. Three hundred and eighty-six cross-peaks in the NOESY ($\tau_{\text{m}} = 100$ ms) spectrum of peptide in DPC were assigned unambiguously. Cross-peak intensities of peptide in DPC were measured in 100 ms NOESY spectrum using the XEASY program. The interproton distance constraints were derived from NOESY cross-peak volumes via ' $1/r^6$ '-calibration, using the CALIBA module of the DYANA program (Guntert *et al.* 1997). Vicinal spin–spin coupling constants $^3J_{\text{HN-C}\alpha\text{H}}$ were determined from the fine structure along the ω_2 axis of the non-overlapped NOESY cross-peaks between the corresponding amide proton (at the ω_2 frequency) and any proton of other residues (at the ω_1 frequency). $^3J_{\text{HC}\alpha\text{-C}\beta\text{H}}$ values were measured in DQF-COSY or TOCSY ($\tau_{\text{m}} = 40$ ms) spectra. Torsion angle constraints were derived from spin–spin

coupling constants and local nuclear Overhauser enhancement (NOE) distance constraints using GRIDSEARCH module of the DYANA program (Guntert *et al.* 1997).

Structure calculation. Spatial structure calculation of hERG S5–P linker peptide in DPC was performed using the DYANA program (Guntert *et al.* 1997). Twenty best structures were selected based on the criterion of small DYANA target function out of 100 calculated structures conforming to experimental constraints. Hydrogen bonds were identified from an analysis of these structures using distance and angle criteria (Baker & Hubbard, 1984). Visual analysis of structures and preparation of figures were performed using the MOLMOL program (Koradi *et al.* 1996).

Mutagenesis and oocyte voltage clamp experiments

The cysteine mutations of the hERG channel have been described before (Liu *et al.* 2002). Oocytes were isolated from *Xenopus laevis*. Animal usage is reviewed annually, and approved, by the Institutional Animal Care and Use Committee of Virginia Commonwealth University. Isolated oocytes were incubated in an ND96-based medium (mM: NaCl 96, KCl 2, CaCl_2 1.8, MgCl_2 1, Hepes 5, sodium pyruvate 2.5, pH 7.5, supplemented with 10% horse serum and penicillin/streptomycin) at 16°C. Five to twelve hours after isolation, each oocyte was injected with cRNA solution using a Drummond digital micro-dispenser. Oocytes were incubated in the above medium at 16°C, and studied 2–4 days after cRNA injection. Membrane currents were recorded from whole oocytes using the '2-cushion pipette' voltage clamp method in a low-Cl ND96 solution (Cl^- in ND96 replaced by methanesulphonate) to reduce interference from endogenous Cl^- channels (Schreibmayer *et al.* 1994). Voltage clamp was done at room temperature (24–26°C) with OC-725B or OC-725C amplifier (Warner Instruments, MA, USA). Voltage clamp protocol generation and data acquisition were controlled by pCLAMP5.5 via a 12-bit D/A and A/D converter (DMA, Axon Instruments, Union City, CA, USA). Current data were low-pass filtered at 1 kHz (Frequency Devices Inc., Haverhill, MA, USA) and stored on disks for off-line analysis. CdCl_2 stock solution (1, 10 or 100 mM) was added to the bath solution to reach desired final concentrations (0.2–100 μM).

Immunoblot and immunocytochemistry

Oocytes were injected with cRNA and incubated as described above. Three days after cRNA injection, oocytes (15–25 oocytes per group) were incubated with 20 mM *N*-ethylmaleimide (NEM) in Tris–EDTA (TE) buffer containing protease inhibitor cocktail (Sigma) at room temperature for 15 min. Oocytes were then homogenized

with a loose-fit glass grinder on ice. The homogenates were centrifuged at 3000 g for 15 min to remove debris, and the supernatants were overlaid on 15% sucrose cushion (in TE buffer containing 20 mM NEM and protease inhibitor cocktail) and centrifuged at 175 000 g for 75 min at 4°C. The pellets (enriched membrane fractions) were resuspended in phosphate-buffered saline (PBS) containing 103 mM KCl and protease inhibitor cocktail and solubilized by incubating with 1% SDS at room temperature for 2 h followed by sonication. Each sample was divided into two aliquots. One was added 2× sample buffer containing 125 mM DTT (reducing) and the other was added 2× sample buffer without DTT (non-reducing) Both were boiled for 5 min before loading on non-reducing SDS–5% polyacrylamide gel. After electrophoresis, proteins were blotted onto a polyvinylidene difluoride (PVDF) membrane (Amersham, Piscataway, NJ, USA). The PVDF membrane was blocked in PBS with 5% non-fat dried milk–0.1% Tween 20 for 1 h at room temperature and then incubated with anti-erg1 antibody (Alomone Labs Ltd, Jerusalem, Israel) at 4°C overnight. This was followed by three 10 min rinses in PBS with 0.1% Tween 20. The membrane was then incubated with alkaline phosphatase-conjugated

secondary antibody (Amersham) for 1 h at room temperature. Immunoreactivity was visualized using an enhanced-chemiluminescence (ECL) detection kit (Amersham).

Oocytes injected with cRNAs or uninjected control oocytes were frozen in Optimal Cutting Temperature compound (OCT). Thin (10- μ m) sections were cut with a cryostat, fixed in 4% formaldehyde, permeabilized with 2% Triton X-100, blocked by 4% goat serum, incubated with anti-erg1 antibody (Alomone), rinsed, incubated with an Alexa 568-conjugated anti-rabbit antibody (Molecular Probes, Eugene, OR, USA), mounted with ProLong antifade agent (Molecular Probes), and viewed using a Zeiss 510 confocal microscope.

Results

Using circular dichroism (CD) and nuclear magnetic resonance (NMR) spectroscopy to study the structure and side chain mobility of the hERG S5–P linker

A synthetic peptide corresponding to amino acids 578–603 of hERG was used in these experiments. CD spectra in Fig. 2A indicate that this hERG S5–P linker peptide was

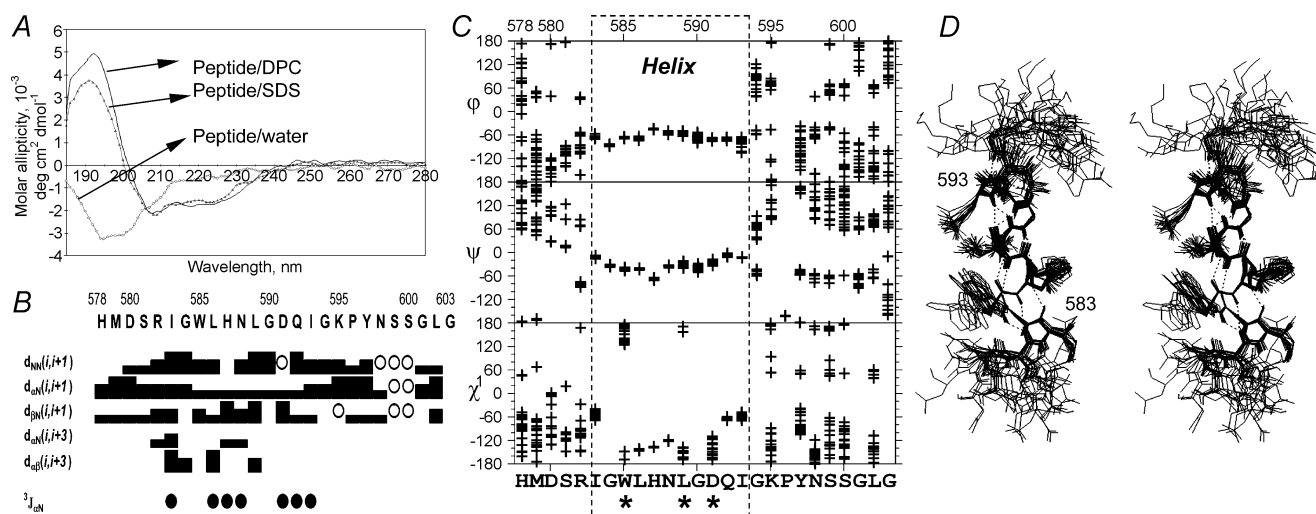


Figure 2. Structures of a hERG S5–P linker peptide corresponding to hERG residues 578–603

A, circular dichroism spectra of the peptide in pure aqueous solution, and in DPC or SDS micelles (peptide concentration 74 μ M, DPC : peptide = 60 : 1, SDS : peptide = 80 : 1, pH 3.5, 22°C). **B**, overview of NMR data defining the secondary structure of the peptide in DPC micelles (peptide concentration 0.6 mM, DPC : peptide = 60 : 1, pH 3.5, 30°C). NOE connectivities are designated as $d_{AB}(i,j)$: connectivity between protons A and B (N, α and β denote the amide, H^α and H^β protons) located in amino acid residues i and j , respectively. Full-size square denotes high intensity, half-size square medium, and line small intensity of corresponding cross peak in NOESY 100 ms spectrum. \circ denote overlapped cross-peaks. $^3J_{NH}$ coupling constants are shown as \bullet , if lower than 5.5 Hz. Peptide sequence along with hERG residue numbers is shown on top. **C**, scatter plot of peptide bond torsion angles (ϕ and ψ) and side chain torsion angles (χ^1) for the 20 best DYANA structures of the peptide in DPC micelles. Peptide sequence is shown at the bottom, and hERG position numbers are shown on top. Dashed box denotes the helix region (583–593), and * marks W585, L589 and D591 in the helix region with flexible side chain orientation. **D**, stereoview of the 20 best structures of the hERG S5–P linker peptide in DPC micelles superimposed on the backbone atoms of the 583–593 region. Backbone and side chain heavy atoms of the 580–596 region are shown. Hydrogen bonds, detected in more than 10 of the 20 best structures, are shown as dotted lines.

unstructured in a pure aqueous solution, but possessed ~30% helical structure in detergent micelles (DPC or SDS). Figure 2B summarizes NMR data used to locate the peptide's helical structure when placed in DPC micelles. Spatial structure calculations showed that the N-terminal (corresponding to hERG residues 578–582) and the C-terminal (594–603) regions were unstructured. However, the segment from 583 to 593 was helical, with 583–590 forming an α -helix and 591–593 forming a 3_{10} helix (Fig. 2C and D). Although we cannot rule out the possibility of solvent-induced formation of an α -helical structure, the NMR analysis in conjunction with our previous functional data (Liu *et al.* 2002) makes a compelling case for the notion that in a functional hERG channel the 583–593 segment can form an α -helix at least in some gating states of the channel.

This helix is amphipathic, with one face occupied by hydrophobic residues (W585, L586, L589 and I593) and the other face occupied by hydrophilic residues (H587, N588, D591 and Q592). The conformations of all side chains in the helical region have been unambiguously determined. Higher dispersion in χ^1 values for W585 and L589, as well as D591, indicates that these side chains may have increased mobility (Fig. 2C).

Western blot analysis reveals that cysteine side chains introduced into the 583–597 segment can form intersubunit disulphide bonds

Cysteine side chains introduced into all positions in the 583–597 segment (excluding non-functional K595C) can spontaneously form disulphide bonds (Liu *et al.* 2002). Where are their 'partner' cysteine side chains? To answer this question, we first needed to determine whether these introduced cysteine side chains form inter- or intra-subunit disulphide bonds. Figure 3A depicts possible scenarios. An introduced cysteine may form a disulphide bond with its counterpart or a native cysteine from a neighbouring subunit (intersubunit disulphide, forming a dimer of ~254 kDa), or with a native cysteine from the same subunit (intrasubunit disulphide, remaining as monomer of ~127 kDa). To determine the nature of disulphide bonds formed by the cysteine side chains introduced into the 583–597 segment, we applied Western blot analysis to channel proteins expressed in oocytes. To avoid non-specific disulphide bond formation, live oocytes were treated with 20 mM NEM to protect free thiol groups before homogenization (see Methods). Oocyte homogenization and membrane fraction isolation were carried out under non-reducing conditions. The final product was divided into two aliquots, one treated with DTT and the other maintained in non-reducing condition, to test whether DTT can alter the banding pattern of channel proteins on the Western blot.

Figure 3B shows a composite image combining five Western blots, where cysteine-substituted mutants along with WT hERG and other negative or positive controls are included for comparison. Membrane protein from control uninjected oocytes (–cRNA) did not show any immunoreactivity to the hERG antibody (2 right-most lanes). The WT hERG protein migrated to a location expected for the monomer. It is a doublet representing glycosylated and core-glycosylated forms (Zhou *et al.* 1998). The banding pattern of WT hERG protein was not altered by DTT treatment, indicating that native cysteines in hERG do not form intersubunit disulphide bonds. Functional data suggest that two cysteine mutants in the S5–P linker outside the 583–597 segment, H578C and T613C, are not capable of forming disulphide bonds (Liu *et al.* 2002; Dun *et al.* 1999). Indeed, both channel proteins migrated to a location expected for hERG monomer, and the banding pattern was not altered by DTT treatment (Fig. 3B, H578C and T613C lanes). It has been shown for the Shaker channel that cysteine substitution at a pore entrance position (M448C) can form intersubunit disulphide bonds (Liu *et al.* 1996). Cysteine substitution at a similar (although not equivalent) pore-entrance position in the hERG channel (S631C) can also form disulphide bonds (Fan *et al.* 1999). Figure 3B shows that under non-reducing conditions, the S631C protein migrated as a major monomer band and a faint dimer band. The dimer band disappeared after DTT treatment, supporting the expectation of intersubunit disulphide bond formation between 631C side chains in some channels.

The above controls confirm the validity of using Western blot analysis on channel proteins expressed in oocytes to detect intersubunit disulphide bond formation. For the cysteine-substituted mutants in the 583–597 segment, G590C did not produce sufficient protein for Western blots (3 attempts). Therefore, this mutant, along with the non-functional K595C, was not included in the Western blot experiments. Figure 3B shows that under non-reducing conditions all 13 cysteine-substituted channel proteins migrated as two bands: one dimer band and one monomer band (–DTT, left of each pair of channel lanes). All the dimer bands disappeared after DTT treatment (+DTT, right of each pair of channel lanes). Therefore, cysteine side chains introduced into positions 583–597 (excluding 590 and 595) were all capable of forming intersubunit disulphide bonds.

We used the ratios of dimer:monomer band intensities as an indicator of how readily the introduced cysteine side chains can form intersubunit disulphide bonds, or how stable such intersubunit disulphide bonds are. The data are summarized in Fig. 3C (numbers in parentheses denote numbers of experiments using different batches of oocytes). Overall, there was a trend of decreasing ratio of dimer:monomer band intensities from the N-terminus to the C-terminus of the 583–597

segment (denoted by the dashed curve), although N588C, L589C and Q592C formed stronger dimer bands than suggested by the trend.

Cysteines introduced into four positions along the 583–597 segment can form intersubunit disulphide bonds with their counterparts from neighbouring subunits

We further explored whether the intersubunit disulphide bonds were formed between counterparts of introduced cysteine side chains, or between introduced and native

cysteine side chains. Four positions with a high tendency of dimer formation were chosen for this analysis: 584, 585, 588 and 589. There are a total of 24 native cysteine side chains in each hERG subunit. Among them, five are in the extracellular region or in the transmembrane segments, and thus could potentially form disulphide bonds with the introduced cysteines. These are C445 and C449 in the S1–S2 linker, C555 and C566 in S5, and C643 in S6. All five native cysteines were substituted with alanine, creating a 'Cys-removed' hERG background (labelled as '- Cys background' in Figs 4 and 5). Cysteine side chains were then reintroduced into this Cys-removed background at 584, 585, 588 and 589.

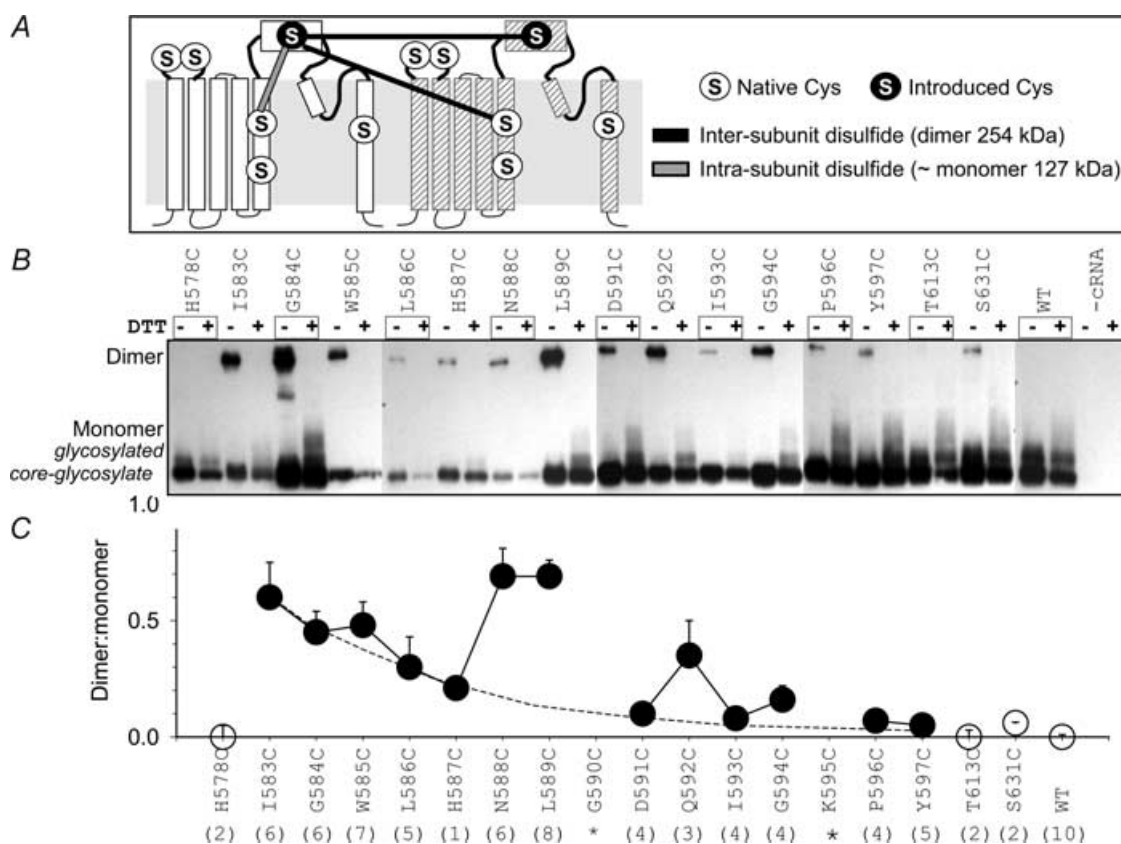


Figure 3. Probing intersubunit disulphide bond formation by Western blot analysis of channel proteins expressed in oocytes

A, diagram of 2 hERG subunits, each marked with an introduced cysteine (Cys) in the S5–P linker and 5 native Cys. The introduced cysteine may form an intersubunit disulphide bond with its counterpart or a native cysteine from a neighbouring subunit (forming a dimer), or an intrasubunit disulphide bond with a native cysteine (molecular size ~ monomer). B, representative Western blot images of membrane proteins prepared from oocytes injected with subunit cRNAs marked on top. '- cRNA' denote uninjected oocytes. Membrane fraction for each channel protein without or with DTT treatment (- or + DTT) was run side-by-side on non-reducing SDS polyacrylamide gels. The positions of dimer and monomer (glycosylated and core-glycosylated forms) are marked on the left. In this and Fig. 5, the amounts of protein loaded in different lanes are not calibrated, causing differences in the overall band intensities. C, ratios of dimer : monomer band intensities determined by densitometry. The monomer band intensities include both glycosylated and core-glycosylated forms. Numbers in parentheses refer to numbers of Western blot measurements from different batches of oocytes. The dashed curve traces the general trend of decreasing dimer : monomer ratio from N- to C-termini.

Although we could detect currents through N588C in the cysteine-removed background (Fig. 4A), for the other channels in the Cys-removed background the current amplitudes were too small to detect even in $98 \text{ mM } [K^+]_o$. Correctly folded channel proteins should be able to pass the quality checkpoint in the endoplasmic reticulum and traffic to the cell surface membrane. Therefore, we used immunocytochemistry in conjunction with confocal microscopy to examine channel protein distribution in oocytes. Figure 4B shows that similar to WT hERG and cysteine-substituted mutants in the WT background, channel proteins in the Cys-removed background, without or with introduced cysteines, all trafficked to the oocyte cell surface. This suggests that channel proteins in the Cys-removed background were correctly folded, and the remaining native cysteine side chains in the cytoplasmic N- and C-terminal domains did not come close to the introduced cysteine side chain in the S5–P linker to interfere with data interpretation. Therefore, we could use these constructs in the Cys-removed background to test

the scenarios depicted in Fig. 5A: if an introduced cysteine side chain forms an intersubunit disulphide bond with any of the native cysteines, this disulphide bond cannot be formed in the Cys-removed background and the protein will migrate as a monomer on a non-reducing SDS gel. On the other hand, a persistent dimer band in the Cys-removed background would indicate that the introduced cysteine side chain can form an intersubunit disulphide bond with its counterpart.

Figure 5B depicts Western blot images of G584C, W585C, N588C and L589C proteins in the Cys-removed background run on a non-reducing gel. The same mutants in the WT background were included as positive control for dimer formation, while the background channel proteins without any introduced cysteines were included as negative control (monomer bands only). All four cysteine-substituted mutants in the Cys-removed background showed clear dimer bands as well as monomer bands, similar to the banding pattern of corresponding cysteine-substituted mutants in the

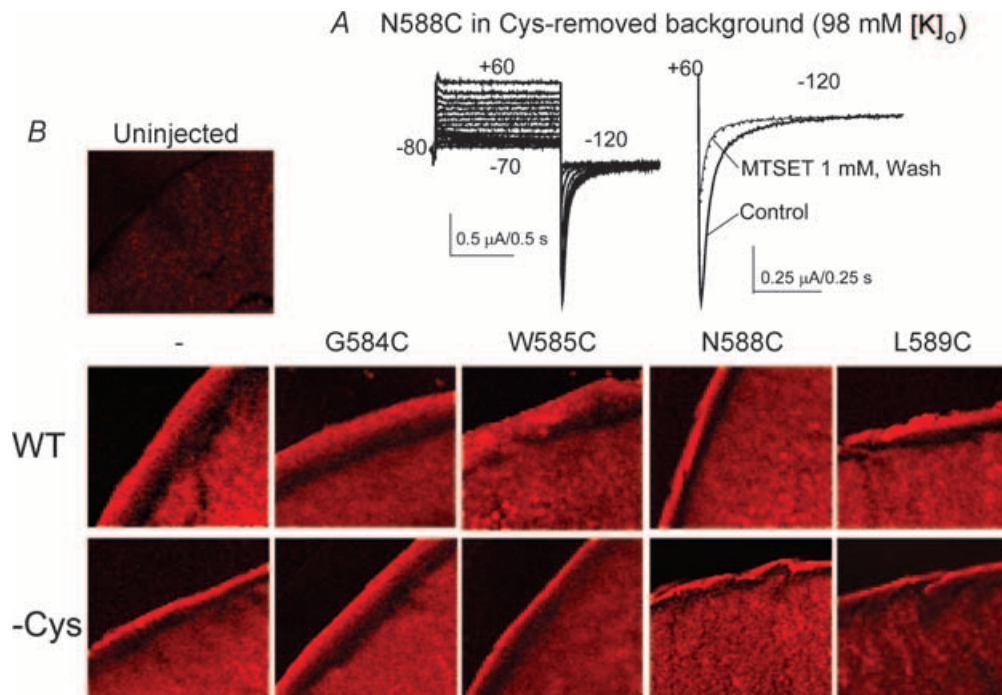


Figure 4. Channel constructs in the Cys-removed (–Cys) background can traffic to the oocyte cell surface Five native cysteines (C445 and C449 in S1–S2 linker, C555 and C566 in S5, and C643 in S6) were replaced by alanine to create the Cys-removed background. Cysteines were then introduced into positions 584, 585, 588, and 589 of this Cys-removed background. *A*, current traces from N588C in the Cys-removed background measured in $98 \text{ mM } [K^+]_o$. Left: family of current traces in response to membrane depolarization from -80 mV to $+60 \text{ mV}$ in 10-mV steps, and repolarizing to -120 mV . Right: irreversible suppressing effects of MTSET on N588C in Cys-removed background, supporting functional channel expression (MTSET does not induce irreversible suppression of oocyte endogenous currents). *B*, testing cell surface expression of WT and mutant hERG channels in oocytes using immunocytochemistry and confocal microscopy. Shown are images of a control (uninjected) oocyte, and oocytes injected with WT or –Cys background without introduced cysteines (marked by ‘–’) or with cysteines introduced into position 584, 585, 588, or 589.

WT background. Similar observations were obtained in multiple experiments (numbers shown in Fig. 5D, from different batches of oocytes). Furthermore, as expected DTT treatment abolished the dimer bands (Fig. 5C). Therefore, cysteine side chains introduced into positions 584, 585, 588 and 589 can form disulphide bonds with their counterparts from neighbouring subunits.

Cysteine side chains at 584, 585, 588 and 589 can coordinate high-affinity Cd²⁺ binding

Disulphide bond formation can trap two cysteine side chains in a bonded state even when the two are apart by as far as 15 Å in flexible proteins (Careaga & Falke, 1992). On the other hand, the formation of a Cd²⁺ bridge has a more stringent requirement for spatial distance between cysteine side chains: distance between C_β atoms should be < 5 Å (Castagnetto *et al.* 2002). Furthermore, the Cd²⁺ affinity depends on the number of thiol side chains that coordinate the Cd²⁺ bridge (Rulisek & Vondrasek, 1998). A tight Cd²⁺ bridge formed between two or more

closely positioned cysteine side chains cannot be broken by removing ambient Cd²⁺ ions. A divalent cation chelator, e.g. EDTA, is needed to remove the bound Cd²⁺ ion. Therefore, to ascertain that cysteine side chains at positions 584, 585, 588 and 589 were indeed close to their counterparts from neighbouring subunits, we tested the effects of Cd²⁺ and the reversibility of these effects upon washout of Cd²⁺ ions. To obtain direct functional readouts under voltage clamp conditions, experiments on G584C, W585C and L589C were conducted using the WT background. For N588C, both WT background and Cys-removed background were studied since both produce sizable currents. This gave us an opportunity to evaluate whether native cysteines play any role in coordinating Cd²⁺ binding to this cysteine-substituted mutant.

Since Cd²⁺ can affect the WT hERG channel (Ho *et al.* 1999; Johnson *et al.* 1999), we first examined the concentration dependence and reversibility of Cd²⁺ effects on WT hERG. WT hERG was not sensitive to 1 μM [Cd²⁺]_o (*n* = 6, one shown in Fig. 6A). At 10 μM, Cd²⁺ accelerated deactivation, shifted V_{0.5} of activation by 15.6 ± 1.2 mV, and modestly reduced the peak amplitude

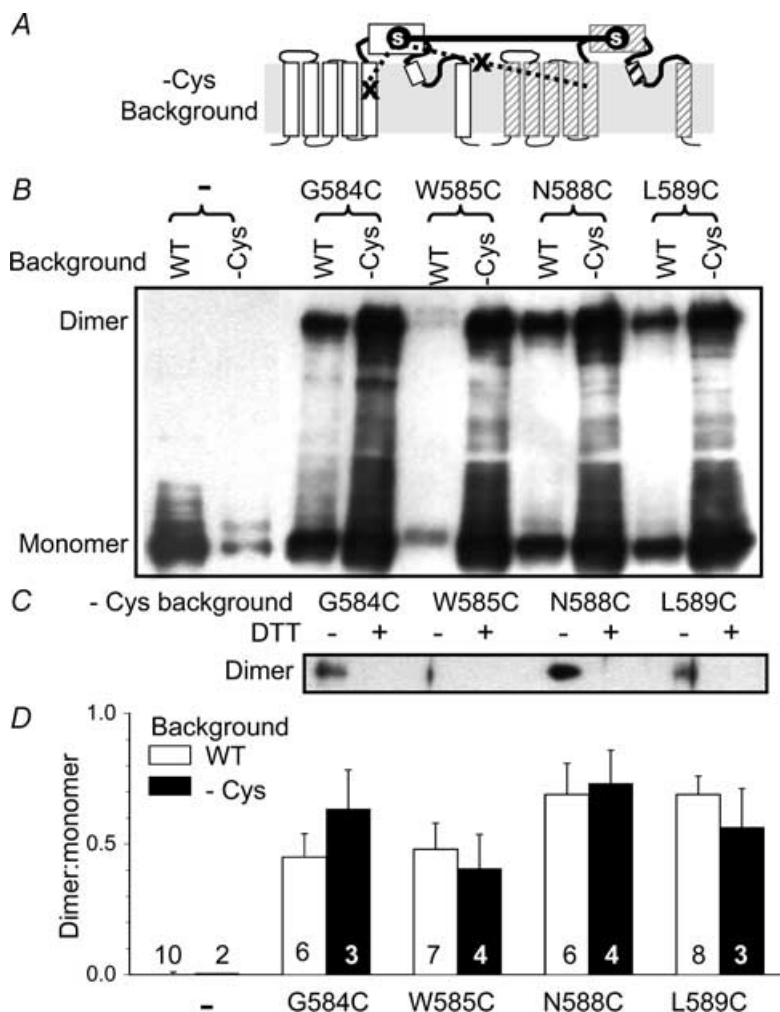


Figure 5. Removing 5 native cysteines from hERG (Cys-removed or '-Cys', background) does not prevent intersubunit disulphide bond formation by 584C, 585C, 588C or 589C

A, schematic diagram of 2 hERG subunits of -Cys background with an introduced cysteine in the S5-P linker. Dimer formation in this background would indicate that an intersubunit disulphide bond is formed between the 2 introduced cysteine residues. B, Western blot images of G584C, W585C, N588C and L589C in the WT background and in the Cys-removed (-Cys) background run on non-reducing gel. Channels without introduced cysteines are also included for comparison (left 2 lanes, marked by '-' on top). Dimer and monomer band positions are marked on the left. C, dimer bands of G584C, W585C, N588C and L589C in the '-Cys background' disappear after DTT treatment. D, ratio of dimer : monomer band intensities of cysteine-substituted mutants in WT or -Cys background (run on non-reducing gels similar to that shown in panel B). Numbers refer to number of Western blot measurements.

of tail currents (by $14 \pm 3\%$, $n = 5$). At $100 \mu\text{M}$, Cd^{2+} suppressed the tail current amplitude by $\sim 70\%$, further accelerated deactivation, and caused a prominent positive shift of $V_{0.5}$ by $\sim 34 \text{ mV}$ ($n = 2$). Even with $100 \mu\text{M}$, these

Cd^{2+} effects on WT hERG were readily reversible upon washing out of Cd^{2+} (Fig. 6A). Therefore, native cysteines in the WT hERG channel were too far apart to coordinate a tight Cd^{2+} binding site on their own.

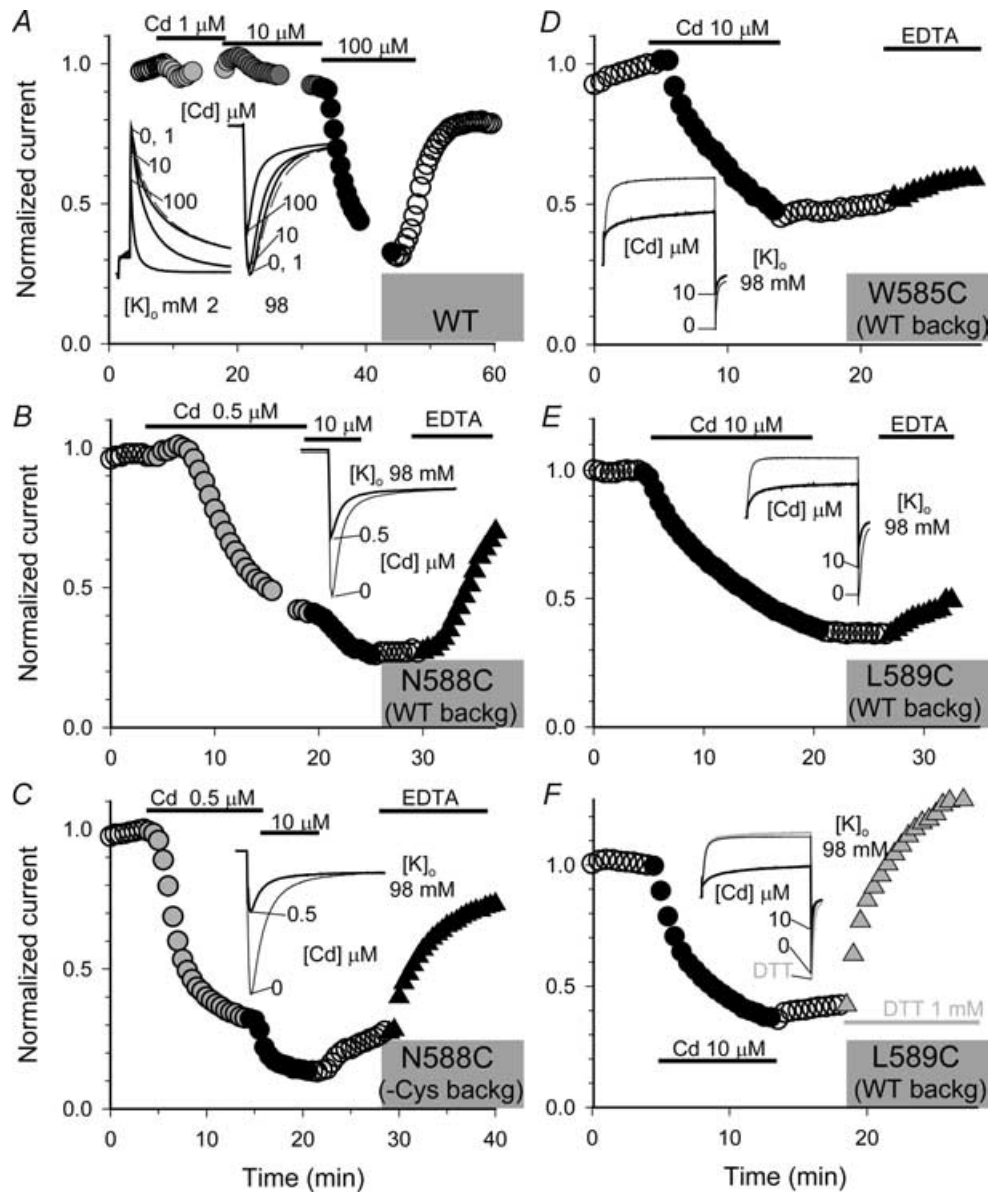


Figure 6. Coordination of high-affinity Cd^{2+} binding by cysteine side chains introduced into positions 585, 588 and 589, but not by native cysteines in WT hERG

Shown in the main graphs are time courses of changes in current amplitude of WT hERG (A), N588C in WT- or Cys-removed background (B and C), W585C and L589C in WT-background (D–F). Channel types are denoted in grey shading areas. Currents were recorded before, during and after exposure to Cd^{2+} of specified concentrations (marked above or below data points) and, for cysteine-substituted mutants, during exposure to 1 mM EDTA (B–E) or 1 mM DTT (F). Oocytes expressing cysteine-substituted mutants were pretreated with DTT, and Cd^{2+} effects were detected after extensive washout of DTT. For cysteine-substituted mutants, recordings were made in 98 mM $[\text{K}^+]_o$ (marked in inset). For WT hERG, the main graph and the left part of the inset were recorded in 2 mM $[\text{K}^+]_o$ while the right part of the inset was recorded in 98 mM $[\text{K}^+]_o$ (marked in inset). Currents were elicited by 1-s depolarization pulses to +60 mV followed by repolarization to –60 mV (WT, in 2 mM $[\text{K}^+]_o$) or –120 mV (WT, in 98 mM $[\text{K}^+]_o$, all cysteine-substituted mutants, in 98 mM $[\text{K}^+]_o$). Current amplitudes were quantified by the peak of tail currents and normalized by the control current amplitude in each experiment. Insets: selected current traces from the same experiments as shown in the main graphs. Shown are either tail currents only (WT in 98 mM $[\text{K}^+]_o$ (A), and N588C (B–C) or both test pulse currents and tail currents.

Figure 6B shows that Cd^{2+} at $0.5 \mu\text{M}$ reduced the current amplitude of N588C in the WT background to 40% of control. Increasing $[\text{Cd}^{2+}]$ to $10 \mu\text{M}$ further decreased the current to 20%. Washout of Cd^{2+} did not reverse the suppression effect, while adding EDTA 1 mM to the bath solution induced a rapid reversal of current suppression. Similar observations were obtained in six experiments. The estimated IC_{50} for Cd^{2+} suppression of N588C in the WT background was $0.31 \pm 0.09 \mu\text{M}$. Figure 6C shows that N588C in the Cys-removed background was equally sensitive to Cd^{2+} . In this case, there was a limited degree of reversibility after Cd^{2+} washout, but the reversal was much faster and more complete by adding EDTA. The estimated IC_{50} for Cd^{2+} suppression of N588C in Cys-removed background was $0.38 \pm 0.09 \mu\text{M}$ ($n = 5$), not different from that of N588C in WT background ($P = 0.563$). The much higher sensitivity of N588C versus WT hERG to Cd^{2+} is not due to the high $[\text{K}^+]_o$ (98 mM) used during recordings. The inset of Fig. 6A shows that elevating $[\text{K}^+]_o$ to 98 mM did not increase the sensitivity of WT hERG to Cd^{2+} . These data indicate that cysteine side chains introduced into position 588 can come very close to counterparts in neighbouring subunits to coordinate a high-affinity Cd^{2+} binding site, and native cysteines are not involved in Cd^{2+} binding.

Cysteine side chains introduced into another position on the hydrophilic face of the S5–P helix, 584, could also coordinate a high-affinity Cd^{2+} binding site (Fig. 7). The effects could not be reversed by washing out Cd^{2+} , but required EDTA to chelate the bound Cd^{2+} ions. The potency of Cd^{2+} to suppress G584C appeared independent of $[\text{K}^+]_o$ ($\text{IC}_{50} = 0.65 \pm 0.08 \mu\text{M}$ and $1.69 \pm 0.81 \mu\text{M}$, in 98 and 2 mM $[\text{K}^+]_o$, respectively, $n = 4$ each, $P = 0.343$).

Figure 6D and E shows that cysteine side chains introduced into positions 585 and 589 on the hydrophobic face of the S5–P helix could also coordinate Cd^{2+} binding, although the binding affinity was lower than that of Cd^{2+} binding to N588C or G584C: IC_{50} was $9.38 \pm 1.42 \mu\text{M}$ for W585C ($n = 6$) and $9.44 \pm 2.43 \mu\text{M}$ for L589C ($n = 11$). There was little or no reversal after washing out Cd^{2+} . However, unlike the situation with N588C and G584C, EDTA did not induce reversal of the Cd^{2+} effect. Instead, DTT could reverse the suppression effect (Fig. 6F, similar observations are obtained in two experiments on W585C and three experiments on L589C). These observations suggest that after Cd^{2+} removal, the apposed 585C or 589C side chains readily form disulphide bonds.

Discussion

The major findings in this study can be summarized as follows. In the hERG channel, cysteine side chains introduced into positions along the 583–597 segment of the S5–P linker (excluding 590 and 595) can form

intersubunit disulphide bonds, leading to a disruption of the fast-inactivation process and a loss of K^+ selectivity. Importantly, cysteine side chains introduced into four of the positions, 584, 585, 588 and 589, can form intersubunit disulphide bonds with their counterparts from neighbouring subunits. They can also coordinate high-affinity Cd^{2+} binding, further confirming their proximity in 3-D space. Circular dichroism and NMR data of a hERG S5–P linker peptide also support the dynamic nature of conformation of the 583–597 segment: it is unstructured in a pure aqueous solution but assumes a helical structure (from positions 583–593, termed ‘S5–P helix’ in the following text) when it comes into contact with a hydrophobic environment.

NMR structures of the isolated S5–P linker peptide: implications for the S5–P linker structure in a functional hERG channel in the cell membrane

Our NMR analysis indicates that the hERG S5–P linker peptide (residues 578–603) can adopt a helical structure in its central portion, with residues 583–590 forming an α -helix and residues 591–593 forming a 3_{10} helix. This prediction is similar, although not identical, to a previous NMR analysis of a longer hERG S5–P peptide (residues 570–611) (Torres *et al.* 2003). The CD data suggest that if the hERG S5–P linker is completely immersed in the extracellular aqueous phase, it is likely to be unstructured. When it is in detergent micelles that mimic the cell membrane environment, it can adopt a helical structure. Our previous functional data suggested that the 583–594 segment has a helical structure (Liu *et al.* 2002). However, in a functional channel the hERG S5–P linker is not likely to be embedded in the membrane lipid bilayer. This casts doubt as to whether the S5–P linker can adopt an α -helical structure in a functional channel. The putative S5–P helix has a hydrophobic face occupied by high-impact positions (W585, L586, L589 and I593) and a hydrophilic face occupied predominantly by intermediate-impact positions (H587, N588, D591 and Q592) (Fig. 8A). It is possible that in a functional channel the central portion of the S5–P linker forms an amphipathic helix lying in the interface between hydrophilic extracellular aqueous solution and hydrophobic channel protein surface, with the hydrophobic residues on the S5–P helix interacting with channel surface domains to stabilize the α -helical structure. Such intimate interactions between channel domains are consistent with the ‘high-impact position’ status of these hydrophobic residues on the S5–P helix (Fig. 8A). In this scenario, the hydrophilic residues face the extracellular aqueous solution, where cysteine substitution has little effects on channel function. However, MTSET modification of these cysteine side chain can reduce current amplitude, or in the

case of G584C, disrupt the fast-inactivation process and the pore's K^+ selectivity. Since cysteine side chains at the intermediate-impact positions can also form disulphide bonds, the hydrophilic face of the S5-P helix must be able to transiently interact with other channel domains or its counterparts in some gating conformations. Taken together, our data suggest that the S5-P linker is not a static structure. Instead, the S5-P helix may rotate around its long axis to allow disulphide bond formation along both its hydrophobic and hydrophilic faces. These helices may also swing along the channel surface to allow cysteine

side chains at positions 584, 585, 588 and 589 to come close to their counterparts to form disulphide bonds or coordinate high-affinity Cd^{2+} binding (distance between $C\beta$ atoms $< 5 \text{ \AA}$).

Do cysteines introduced into positions 584, 585, 588, and 589 form intersubunit disulphide bonds with counterparts from adjacent or diagonal subunits?

Our previous data suggest that the N-terminus of the S5-P helix is close to the pore entrance and to counterparts from

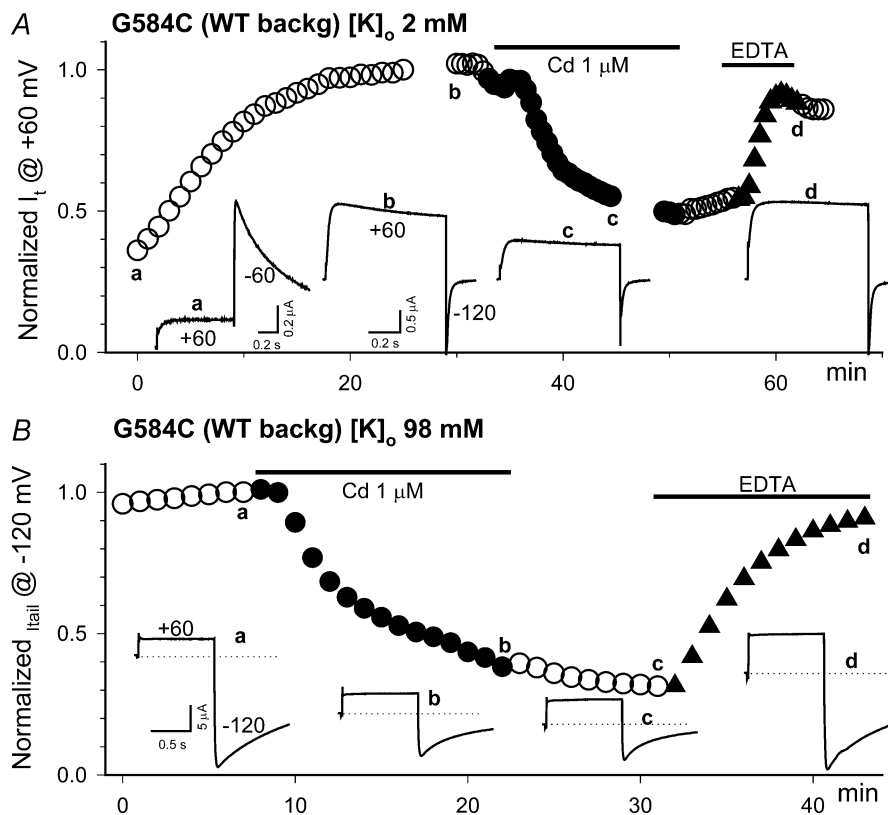


Figure 7. Coordination of Cd^{2+} binding by cysteine side chains at position 584 detected in 2 mM $[K^+]_o$ (A) or 98 mM $[K^+]_o$ (B)

Shown in the main graphs are time courses of changes in G584C (in WT background) current amplitude recorded from oocytes pretreated with DTT. During recording, oocytes were superfused with DTT-free bath solution. Duration of exposure to Cd^{2+} ($1 \mu M$) or EDTA ($1 mM$) is denoted by filled circles or triangles, respectively, as well as by horizontal lines above data points. Insets: representative current traces from the same experiments as shown in the main graphs at time points 'a'–'d'. In both experiments, the channels were activated by 1-s pulses to +60 mV. In the experiment conducted in 2 mM $[K^+]_o$ (A), the repolarization voltage was -60 mV initially, when G584C was in 'WT-like' behaviour after DTT treatment (small test pulse current at +60 mV and large outward tail current at -60 mV) (Liu *et al.* 2002). However, after continuous pulsing while being superfused with DTT-free bath solution, the G584C channels gradually switched to the mutant behaviour (outward shift of test pulse current at +60 mV, reduced K^+ selectivity and positive shift in reversal potential) (Liu *et al.* 2002). The repolarization voltage was switched to -120 mV because under these conditions tail currents became inward at voltages below the activation threshold (-50 mV) and were very small at -60 mV. In the experiment conducted in 98 mM $[K^+]_o$ (B), the repolarization voltage was maintained at -120 mV throughout the protocol. There were sizable inward tail currents at -120 mV during the whole period, although whether there was any degree of phenotype switch is not clear. The dotted lines denote current level during a brief prepulse (before channel activation) to -120 mV, that served as baseline for measuring the peak tail current amplitudes at -120 mV.

other subunits (Liu *et al.* 2002). We also propose that the S5–P helix is orientated with its C-terminus pointing away from the pore entrance. This arrangement is consistent with the trend of intersubunit disulphide bond stability suggested by Fig. 3C: the N-terminal end of S5–P helix is closer to each other than the C-terminal end and can more readily form intersubunit disulphide bonds. If the S5–P helices are arranged around the central pore in 4-fold symmetry, then the distance between cysteine side chains at equivalent positions on the S5–P helices is shorter between adjacent subunits than between diagonal subunits. Although we do not have high-resolution data to definitely conclude one way or the other, the available information does suggest that these cysteine side chains are more likely to form intersubunit disulphide bonds with counterparts from adjacent subunits than from the diagonal subunit. Data from G584C also support this scenario. This channel manifests WT-like behaviour when the thiol side chains are in reduced state, but switches to the mutant behaviour (disruption of fast inactivation and K⁺ selectivity) when the thiol side chains form disulphide bonds. Therefore, we can track disulphide bond formation during the course of an experiment. Figure 7A shows that after DTT washout, G584C gradually switches to the mutant behaviour, indicating disulphide bond formation. This process of ‘phenotype-switch’ reaches a steady state in about 30 min.

Adding Cd²⁺ 1 μM at this point can effectively suppress the current, and washing out Cd²⁺ does not reverse the suppressing effect until EDTA is applied. This indicates that Cd²⁺ is coordinated by at least two cysteine side chains in close proximity (although histidine side chains can also coordinate Cd²⁺ ions). Although this observation represents the averaged behaviour of all G584C channels in the oocyte cell membrane, the data are consistent with the notion that disulphide bonds are formed between 584C from two adjacent subunits (thus allowing current through the pore). Furthermore, formation of one disulphide bond within a channel between two adjacent subunits does not perturb the outer mouth conformation significantly, so that the remaining two free thiol groups can still coordinate a high affinity Cd²⁺ binding site.

Why is the S5–P linker so critical for the fast-inactivation process of the hERG channel?

In Fig. 8B, we propose three models for how S5–P helices in a functional hERG channel interact with each other, and how these S5–P helices may contribute to the channel’s fast-inactivation process. Although a transition of the S5–P linker conformation between helical and coil is possible during hERG gating, this possibility is not included in the

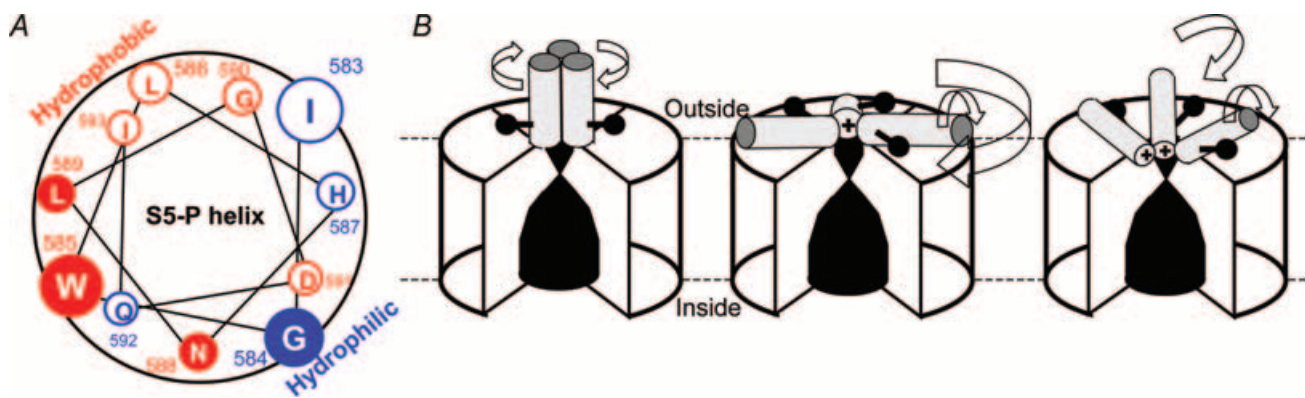


Figure 8. Working models for the structure–function relationship of S5–P helices in the hERG channel

A, helical wheel plot of hERG’s S5–P helix (residues 583–593), viewed from the N-terminus, with residues closer to the viewer drawn larger than those closer to the C-terminus. The hydrophobic and hydrophilic faces are marked. High- and intermediate-impact positions are colour coded red and blue, respectively. The 4 positions where cysteine substitution can form intersubunit disulphide bonds with counterparts are highlighted by white lettering on coloured background. B, three models of S5–P helix orientation and possible role in the inactivation process of the hERG channel. Channels are shown in cell membrane (boundaries denoted by dashed lines) with extracellular domains on top. The subunit closer to the viewer is removed to reveal the putative relationship between the S5–P helices and the pore, which has a narrow selectivity filter and a large inner cavity. Cylinders represent S5–P helices, with their N-termini juxtaposed to the pore entrance with positive signs to denote the helical dipole potential. The ball-and-sticks represent cysteine side chains introduced into the S5–P helices that can form intersubunit disulphide bonds with counterparts from adjacent subunits. Arrows denote molecular motions of the S5–P helices needed to allow cysteine side chains at equivalent positions from adjacent subunits to form intersubunit disulphide bonds. For more discussion, see text.

simplified models depicted in Fig. 8B. In the left panel of Fig. 8B, the S5–P helices are orientated perpendicular to the plane of the cell membrane. Relatively small asymmetric rotations of S5–P helices along their long axes can allow intersubunit disulphide bond formation between cysteine side chains at equivalent positions from adjacent or even diagonal subunits. These S5–P helices come close to each other during channel inactivation, preventing K⁺ ion flux through the pore by steric hindrance or by a hydrophobic seal formed between hydrophobic residues along the S5–P helices. In the middle panel, the S5–P helices are orientated parallel to the plane of the cell membrane. Asymmetric rotations of S5–P helices along their long axes, as well as relatively large-scale sideways swinging motion along the channel surface, are needed to allow cysteine side chains at equivalent positions of adjacent subunits to form intersubunit disulphide bonds. Channel inactivation occurs when all four helices point their N-terminal positive helical dipole (Hol, 1985) toward the pore entrance, creating a local electrostatic potential unfavourable to K⁺ ion flux through the pore. In the right panel, the S5–P helices are tilted and sink into the channel pore to interact with the selectivity filter. Asymmetric rotations along their long axes as well as small-scale sideways swinging are needed to allow intersubunit disulphide bond formation between cysteine side chains at equivalent positions of adjacent subunits. Channel inactivation is envisioned to be due to two factors: (a) local electrostatic potential due to the N-terminal positive helical dipole of the four S5–P helices (Hol, 1985), and (b) interactions between the S5–P helices and the pore-loops, causing conformational changes around the selectivity filter that shut down K⁺ flux through the pore.

The advantage of the first model is that relatively small molecular motions can allow intersubunit disulphide bond formation between counterparts from adjacent or diagonal subunits. However, the disadvantage of this model is that it does not explain how the S5–P helices are stabilized in an aqueous environment. In the second and third models, the S5–P helices are stabilized by the interaction between residues on its hydrophobic face and the channel surface domain. The third model has the added advantages over the second model in that smaller sideways swinging motion allows intersubunit disulphide bond formation between cysteines at equivalent positions of two adjacent subunits, and the proposed interaction between the S5–P helix and the pore loop can better explain why the pore's K⁺ selectivity is disrupted by mutations at high-impact positions along the S5–P helix. We have proposed that relative to the Shaker channel, there are fewer hydrogen bonds formed between residues around the outer mouth of the hERG channel (Fan *et al.* 1999). This may result in a

'floppy' outer mouth structure, able to accommodate the insertion of the S5–P helices as proposed in the third model.

Technical consideration: validity of using cysteine-substituted mutants or cysteine-removed background channels to probe the structure–function relationship of hERG's S5–P linker

A critical issue for data interpretation in these experiments is whether the cysteine-substituted mutants maintain the native conformation of the channel's outer vestibule. This is the case for cysteine substitution at intermediate-impact positions, because these channels maintain the WT phenotype as long as the thiol side chains are in the reduced state. For cysteine substitution at the high-impact positions, although the inactivation process and K⁺ selectivity are disrupted even when the thiol side chains are reduced, 5 of the channels (L586C, N588C, L589C, D591C and I593C) maintain a high sensitivity to a peptide toxin, ErgTx1, similar to that of the WT hERG channel (mean IC₅₀ range 2.3–10.7 nM, *versus* 7.2 nM for WT hERG) (Pardo-Lopez *et al.* 2002). Since such a high toxin binding affinity requires the maintenance of multiple contact points between toxin and the channel's outer vestibule, the data argue that these five cysteine-substituted mutants at the high impact positions do not drastically alter the outer mouth conformation. The remaining two cysteine substituted mutants (W585C and G590C) manifest markedly reduced ErgTx1 binding affinity (IC₅₀ > 100 nM) (Pardo-Lopez *et al.* 2002). They are therefore less informative because of the uncertainty as to whether they maintain the native conformation of the outer vestibule.

Currents through channels in the Cys-removed background (5 native cysteines replaced by alanines, Fig. 4 legend) are very small or not detectable. This is likely to be due to the removal of C566 in S5, because removing the other four native cysteines, singly or in combination, does not significantly reduce the current amplitude (data not shown). Although the mechanism for the detrimental effect of C566A on hERG channel function is not clear, we argue that the transmembrane topology of channels in the Cys-removed background is maintained as the WT hERG. This is based on the observation that channels in the Cys-removed background can traffic to the oocyte cell surface, similar to channels in the WT background (Fig. 4B). This is possible only if these channel proteins are correctly folded so that they can exit the ER checkpoint. It is important to point out that in the oocyte Western blot experiments, all free thiol groups in intact and functional channels are blocked by 20 mM NEM before homogenization (see Methods). Disulphide bonds detected in Western blot experiments represent those formed in the

in situ intact channels. Therefore, our data rule out the possibility that for channels in the Cys-removed background the remaining native cysteine side chains (in the cytoplasmic domain) can form disulphide bonds with those cysteine side chains introduced into the extracellular S5-P linker and interfere with data interpretation.

Our data cannot distinguish between two possibilities: cysteine side chains introduced into the 583–597 segment form disulphide bonds with specific partners, or with multiple partners in different gating conformations. In the Shaker channel, cysteine side chains introduced into several positions in S4 can form disulphide bonds with cysteine introduced into the same position of S5 in a gating state-dependent manner (Gandhi *et al.* 2003). Furthermore, whether cysteines introduced into positions other than 584, 585, 588 and 589 can form intersubunit disulphide bonds with counterparts from neighbouring subunits needs to be tested.

References

- Baker EN & Hubbard RE (1984). Hydrogen bonding in globular proteins. *Prog Biophys Mol Biol* **44**, 97–179.
- Bartels C, Xia TH, Billeter M, Guntert P & Wuthrich K (1995). The program XEASY for computer-supported NMR spectral analysis of biological macromolecules. *J Biomol NMR* **6**, 1–10.
- Bax A & Davis DG (1985). MLEV-17-based two-dimensional homonuclear magnetization transfer spectroscopy. *J Magn Reson* **65**, 355–366.
- Careaga CL & Falke JJ (1992). Thermal motions of surface α -helices in the D-galactose chemosensory receptor. Detection by disulfide trapping. *J Mol Biol* **226**, 1219–1235.
- Castagnetto JM, Hennessy SW, Roberts VA, Getzoff ED, Tainer JA & Pique ME (2002). MDB: the metalloprotein database and browser at the Scripps Research Institute. *Nucl Acids Res* **30**, 379–382.
- Doyle DA, Cabral JM, Pfuetzner RA, Kuo A, Gulbis JM, Cohen SL, Chait BT & MacKinnon R (1998). The structure of the potassium channel: molecular basis of K^+ conduction and selectivity. *Science* **280**, 69–77.
- Dun W, Jiang M & Tseng G-N (1999). Allosteric effects of mutations in the extracellular S5-P loop on the gating and ion permeation properties of hERG. *Pflugers Arch* **439**, 141–149.
- Fan J-S, Jiang M, Dun W, McDonald TV & Tseng G-N (1999). Effects of outer mouth mutations on hERG channel function: a comparison with similar mutations in Shaker. *Biophys J* **76**, 3128–3140.
- Gandhi CS, Clark E, Loots E, Pralle A & Isacoff EY (2003). The orientation and molecular movement of a K^+ channel voltage-sensing domain. *Neuron* **40**, 515–525.
- Guntert P, Mumenthaler C & Wuthrich K (1997). Torsion angle dynamics for NMR structure calculation with a new program DYANA. *J Mol Biol* **273**, 283–298.
- Herzberg IM, Trudeau MC & Robertson GA (1998). Transfer of rapid inactivation and sensitivity to the class III antiarrhythmic drug E-4031 from HERG to M-eag channels. *J Physiol* **511**, 3–14.
- Ho W-K, Kim I, Lee CO, Youm JB, Lee SH & Earm YE (1999). Blockade of HERG channels expressed in *Xenopus laevis* oocytes by external divalent cations. *Biophys J* **76**, 1959–1971.
- Hol WG (1985). Effects of the alpha-helix dipole upon the functioning and structure of proteins and peptides. *Adv Biophys* **19**, 133–165.
- Hoshi T, Zagotta WN & Aldrich RW (1991). Two types of inactivation on Shaker K^+ channels: effects of alterations in the carboxy-terminal region. *Neuron* **7**, 547–556.
- Jeener J, Meier GH, Backman P & Ernst RR (1979). Investigation of exchange processes by two-dimensional NMR spectroscopy. *J Chem Phys* **71**, 4546–4553.
- Jiang Y, Lee A, Chen J, Cadene M, Chait BT & MacKinnon R (2002). Crystal structure and mechanism of a calcium-gated potassium channel. *Nature* **417**, 515–522.
- Jiang Y, Lee A, Chen J, Ruta V, Cadene M, Chait BT & MacKinnon R (2003). X-ray structure of a voltage-dependent K^+ channel. *Nature* **423**, 33–41.
- Johnson JP, Balser JR & Bennett PB (1999). Enhancement of HERG K^+ currents by Cd^{2+} destabilization of the inactivated state. *Biophys J* **77**, 2534–2541.
- Koradi R, Billeter M & Wuthrich K (1996). MOLMOL: a program for display and analysis of macromolecular structures. *J Mol Graphics* **14**, 51–55.
- Liu Y, Jurman ME & Yellen G (1996). Dynamic rearrangement of the outer mouth of a K^+ channel during gating. *Neuron* **16**, 859–867.
- Liu J, Zhang M, Jiang M & Tseng G-N (2002). Structural and functional role of the extracellular S5-P linker in the HERG potassium channel. *J Gen Physiol* **120**, 723–737.
- Pardo-Lopez L, Zhang M, Liu J, Jiang M, Possani LD & Tseng G-N (2002). Mapping the binding site of a HERG-specific peptide toxin (ErgTx) to the channel's outer vestibule. *J Biol Chem* **277**, 16403–16411.
- Rance M, Sorensen OW, Bodenhausen G, Wagner C, Ernst RR & Wuthrich K (1983). Improved spectral resolution in COSY 1H -NMR spectra of protein via double quantum filter. *Biochem Biophys Res Comm* **117**, 479–485.
- Rulisek L & Vondrasek J (1998). Coordination geometries of selected transition metal ions (Co^{2+} , Ni^{2+} , Cu^{2+} , Zn^{2+} , Cd^{2+} , and Hg^{2+}) in metalloproteins. *J Inorganic Biochem* **71**, 115–127.
- Sanguinetti MC, Jiang C, Curran ME & Keating MT (1995). A mechanistic link between an inherited and an acquired cardiac arrhythmia: HERG encodes the I_{Kr} potassium channel. *Cell* **81**, 299–307.
- Schreibmayer W, Lester HA & Dascal N (1994). Voltage clamping of *Xenopus laevis* oocytes utilizing agarose-cushion electrodes. *Pflugers Arch* **426**, 453–458.
- Smith PL, Baukrowitz T & Yellen G (1996). The inward rectification mechanism of the HERG cardiac potassium channel. *Nature* **379**, 833–836.
- Spector PS, Curran ME, Zou A, Keating MT & Sanguinetti MC (1996). Fast inactivation causes rectification of the I_{Kr} channel. *J Gen Physiol* **107**, 611–619.

- Torres AM, Bansal P, Sunde M, Clarke CE, Bursill JA, Smith DJ, Bauskin A, Breit SN, Campbell TJ, Alewood PF, Kuchel PW & Vandenberg JI (2003). Structure of the HERG K⁺ channel S5P extracellular linker: role of an amphipathic α -helix in C-type inactivation. *J Biol Chem* **278**, 42136–42148.
- Wuthrich K (1986). *NMR of Proteins and Nucleic Acids*. Wiley, New York.
- Zhou Z, Gong QYeB, Fan Z, Makielski JC, Robertson GA & January CT (1998). Properties of HERG channels stably expressed in HEK 293 cells studied at physiological temperature. *Biophys J* **74**, 230–241.

Acknowledgements

This work was supported by HL 46451 and HL 67840 from NIH/NHLBI and a grant-in-aid award from AHA/Mid-Atlantic Affiliate (GNT), and by Russian Ministry of Education and Science and Russian Basic Research Foundation. The authors would like to thank Dr H. R. Guy (National Cancer Institute of National Institutes of Health) for helpful discussions along the course of this project.